HOM IDENTIFICATION AND BEAD PULLING
IN THE BROOKHAVEN ERL *

H. Hahn[#,] Wencan Xu, C-AD, Brookhaven National Laboratory, Upton, NY 11973
Puneet Jain, Elliott C. Johnson, Stony Brook University, Stony Brook, NY, 11733

Abstract

Several past measurements of the Brookhaven ERL at superconducting temperature produced a long list of higher order modes (HOMs). The Niobium 5-cell cavity is terminated with HOM ferrite dampers that successfully reduce the Q-factors to tolerable levels. However, a number of undamped resonances with $Q \geq 10^6$ were found at 4 K and their mode identification remained as a goal for this paper. The approach taken here consists in taking different S_{21} measurements on a copper cavity replica of the ERL which can be compared with the actual data and also with Microwave Studio computer simulations. Several different S_{21} transmission measurements are used, including those taken from the fundamental input coupler to the pick-up probe across the cavity, between probes in a single cell, and between beam-position monitor probes in the beam tubes. Mode identification is supported by bead pulling with a metallic needle or a dielectric sphere that are calibrated in the fundamental mode. This paper presents results for HOMs in the first two dipole bands with the prototypical 958 MHz trapped mode, the lowest beam tube resonances, and high-Q modes in the first quadrupole band and beyond.

INTRODUCTION

Several past measurements of the Brookhaven ERL at superconducting temperature produced a long list of higher order modes (HOMs). The Niobium 5-cell cavity is terminated with HOM ferrite dampers that successfully reduce the Q-factors to tolerable levels. However, a number of undamped resonances with $Q \geq 10^6$ were found at 4 K and are listed in Table I. Their mode identification is essential in order to establish the R/Q for beam break up estimates and this task remained as one goal for this paper. The present study was also initiated to prepare for the field flatness measurement and the HOM identification of the BNL-3 cavity that is being constructed for the electron ion collider at Brookhaven, eRHIC. As a preparatory step in developing the best techniques, bead-pull measurements were performed on a copper cavity replica of the ERL and compared with Microwave Studio computer simulations.

This paper is organized as follows. In Section II, the bead-pull technique is described with considerable detail and theoretical sensitivity factors are collected in a table.

Table I: High-Q modes in the BNL ERL @ 4 K

f [GHZ]	Q
1.22008	920,000
2.14764	5,503,500
2.14831	1,306,900
2.32984	2,291,800
2.34421	908,180
2.45578	1,025,400
2.74324	620,040
2.90829	406,090

In Section III, bead pulling with a metallic cylinder and a dielectric sphere is applied to the fundamental TM01-π mode yielding field flatness and a calibration of the beads. Section IV discusses resonances that are located in the bam tube between cavity and ferrite damper and distort the proper cavity modes. A major concern in the cavity design stage and then during the measurements is the existence of trapped modes such as the ~ 958 MHz resonance analyzed in Section V. In the last Section VI, the attempt at identification of the very high-Q resonances using bead-pulling is presented and compared to other methods. The short conclusion summarizes the necessary steps and limitations of HOM identification in the ERL cavity.

PERTURBATION MEASUREMENTS

The availability of advanced electromagnetic computer programs has to some degree replaced perturbation measurements to obtain field configuration and the performance parameters of resonant cavities. However, they remain a valuable tool to analyze geometrically complex structures or to confirm theoretical results that are modified by construction errors. Measurements by bead pulling were performed for this paper in order to verify the field flatness and to identify higher order modes in the copper model of the five-cell ERL cavity in Fig. 1.

The frequency change produced by the insertion of an object into a resonant cavity is a topic in standard electromagnetic text books. The possibility to interpret this frequency change for the identification of the local field strength and direction as well as the cavity interaction parameters was pointed out by Müller [1] and is well known in the accelerator community as Slater perturbation method [2]. Theoretical expressions for the frequency change have been derived for simple geometries with a near complete list to be found in a technical report by L. C. Maier, Jr. [3]. The typical application of bead-bull measurements is to establish or to

confirm field flatness in multi cell linac cavities [4]. If the perturbing object has known properties, then it becomes possible to also determine the interaction parameter R/Q [5]. Bead pulling for Higher Order Mode (HOM) identification in the copper Energy Recovery Linac (ERL) cavity has been discussed previously in Ref [6].
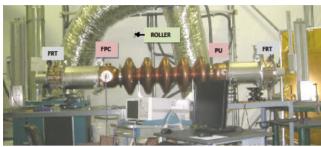

FIG. 1: Copper model of the BNL ERL cavity

The Frequency Shift

The perturbation method consists in measuring, the frequency shift, $\Delta\omega = \omega - \omega_0$ due to the insertion of the perturbing object. The shift is given by the expression involving the local electric and magnetic field strength,

$$\frac{\Delta\omega}{\omega_0} = -F_E \frac{\varepsilon_0 EE^*}{U} + F_H \frac{\mu_0 HH^*}{U}, \qquad (1)$$

where ε_0 and μ_0 are the dielectric and magnetic constants of free space, U is the stored energy in the cavity, and F_E, F_H are geometry factors that quantify the coupling of the perturbation to the E and H fields, respectively. Metallic beads, either as spheres or as "needles" are readily available and produce the largest signal but do not distinguish electric and magnetic fields. Dielectric beads with unknown dielectric constant and metallic needles have to be calibrated for accurate measurements. Most measurements for this paper were performed with thin needle-like cylinders, treated as prolate metallic ellipsoids, that are sensitive to the coaxial electric field and relatively insensitive to the transverse magnetic field components. The dimensionless geometry factors are known for simple geometries and are listed in Table II.

Table II: Perturbation factors ($r/h \ll 1$) [3]

Bead	F_E	F_H
Metallic sphere, (radius r)	πr^3	$\pi r^3 / 2$
Dielectric sphere (radius r)	$\pi r^3 \frac{\varepsilon - 1}{\varepsilon + 2}$	-
Metallic cylinder $\parallel$ field (length h, radius r)	$\dfrac{\pi}{24}\dfrac{h^3}{\ln\frac{h}{r}-1}$	$\dfrac{\pi}{6}\dfrac{h^3}{\frac{h^2}{r^2}-2+4\ln\frac{h}{r}}$
Metallic cylinder $\perp$ field (length h, radius r)	$\dfrac{\pi}{12}\dfrac{h^3}{\ln\frac{h}{r}-\frac{1}{2}+\frac{h^2}{4r^2}}$	$\dfrac{\pi}{12}\dfrac{h^3}{\ln\frac{h}{r}+\frac{h^2}{4r^2}-\frac{5}{2}}$

Needles are appropriate for determining the field flatness in the TM_{01} π mode of the BNL five-cell cavity. HOM mode identification was started with needles and then supported by dielectric beads, but needs to be confirmed with a MWS computer field simulation.

Measurement Techniques

The perturbation frequency shift $\Delta\omega$ in any cavity resonance is found with the network analyzer via the changes in a S_{21} measurement according to the relation

$$S_{21} = |S_{21}|e^{j\Phi} = \frac{2Q_L}{\sqrt{Q_{in}Q_{out}}(1+jQ_L X)} \qquad (2)$$

with $Q_L^{-1} = Q_0^{-1} + Q_{in}^{-1} + Q_{out}^{-1}$ and $X = \omega/\omega_0 - \omega_0/\omega \approx 2\Delta\omega$ In principle, $\Delta\omega$ can be obtained from the peak of absolute $|S_{21}|$ but only as sum of electric and magnetic effect whereas using the phase shift Φ in S_{21} gives the algebraic contribution from electric and magnetic fields separately and is to be preferred,

$$\frac{\Delta\omega}{\omega_0} = \frac{1}{2Q_L}\tan\Phi . \qquad (3)$$

The Experimental Setup

The bead-pulling assembly for the ERL copper model is shown in Fig. 2. The setup consists of a pulley-mounted driver motor moving the perturbing bead on a dielectric filament through the cavity, in X-Y translated runs with precise on and off-axis alignment. Coupling the network analyzer to a resonance can be achieved between the fundamental coupler and the Pick-up probe, or between capacitive probes entered in the end sections or through small holes drilled into the cavity cells.
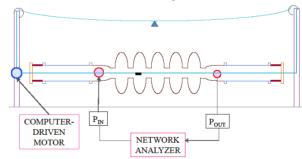

FIG. 2: Bead-Pull experimental Setup

The induced phase shift is obtained by taking the following steps. The network analyzer is set up to sweep across the centered resonance with a defined frequency span, that is chosen to cover the resonance in dB format for the loaded-quality factor measurement and thus depends on the quality factor. The sweep speed is adjusted to match the bead advancement through the cavity, with the IF band width set to 30 Hz. After changing dB to phase format and starting the bead movement, the screen shows the resonance in phase format with the frequency calibrated to the trace number. Finally, the frequency span is set to zero with the bead

removed from the cavity, which establishes the $\Phi = 0$ calibration and the moving bead traces the resonance curve with the phase calibrated to the trace number. Accurate numerical field measurements would be available if Q_L was measured and the bead was calibrated.

FUNDAMENTAL MODE FIELD FLATNESS & BEAD CALIBRATION

A major objective of the present study was preparing for the field flatness tests of the five-cell BNL-3 cavity which is now being constructed. This is realistically done by bead-pull measuring the field flatness in the copper model of the ERL cavity. The first task encountered here is to establish the axial bead position in the cavity with respect to the cells. The fully assembled model shown in Figs. 1 has added short small-aperture extensions resulting in a system length of 298.6 cm. The frequency sweep speed of the NWA was set by selecting a 30 Hz IF to 51.625 sec in order to match it with the time required by the bead to traverse the model. The MWS model for the ERL was adjusted to match the entire full length copper model.
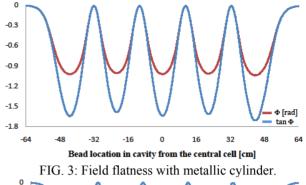
The reference data for the bead pulling was obtained from a simple S_{21} measurement, producing the loaded quality factor, $Q_L \approx 23,200$ and the zero, Φ_0 on the phase curve at the resonance $f_0 = 702.65$ MHz. The reference is established with the bead removed, but must be done with the fish line inserted on axis. Bead pulling for field flatness was done with a metal cylinder and a dielectric sphere to distinguish $|E_X|$ and EE^*. For these measurements, a metallic "needle-like" cylinder (length $h = 17.5$ mm, radius $r = 1.65$ mm) and a dielectric sphere (radius $r = 6.35$ mm) were used as the perturbations.

Field Flatness

The phase shifts generated by cylinder and sphere are shown in Fig. 3 and 4 respectively. The raw data is the phase shift, Φ and it is transformed with $\tan \Phi$ into the frequency shift connected to the field strength. The TM_{01} π- mode is characterized by the longitudinal electric field on the cavity axis. Consequently, the perturbations due to needle and sphere were introduced at the center of the cavities, so that a shift in frequency is produced by the axial electric component of the fields. The frequency shift due to the two available beads extends into the nonlinear region of the phase curve and the application of tan is mandatory here, suggesting using smaller sizes. The field strength follows by taking the square root of the $\tan \Phi$ signal in each cell. The results in normalized units are listed in Table III, yielding an overall flatness of ~2 %.

Table III. Field flatness

Cell #	1	2	3	4	5	<>
Needle	1.238	1.260	1.281	1.272	1.308	1.281 ±0.027
Sphere	1.319	1.293	1.313	1.303	1.343	1.314 ±0.029

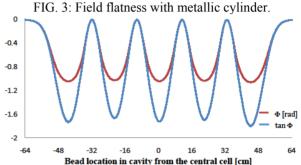FIG. 3: Field flatness with metallic cylinder.

FIG. 4: Field flatness with dielectric sphere.

Bead Calibration

The preceding field flatness measurement produced only a relative value of the electrical field on axis of a known mode. HOM identification requires finding a more general field configuration. This too can be obtained with bead pulling by taking into account the effect of a particular bead on the type and strength of the local field. The bead characteristics enter into the frequency shift measurements through the geometric factors viz. F_E and F_H, defined in the previous section. However, the geometry factor that is transportable for use in another cavity must be calibrated for a specific bead.
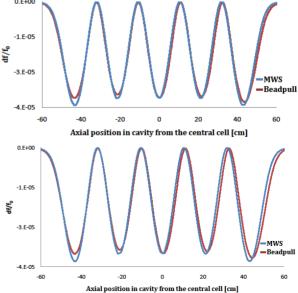

FIG. 5 & 6: *F*-calibration of needle and sphere
$F_H = 6.6E\text{-}7 \text{ m}^3$ and $F_E = 6.93E\text{-}7 \text{ m}^3$.

The bead calibration is done here in the $TM_{01}\pi$ mode by enforcing the relation

$$F_E = (\Delta\omega / \omega)/(\varepsilon_0 EE^* / U) \qquad (4)$$

for which $\varepsilon_0 EE^* / U$ is known from the MWS simulation and the frequency shift is measured by bead pulling together with the loaded Q measurement. Fitting the F-adjusted perturbation curve to the MWS curve is shown in Fig. 5 for the needle and in Fig. 6 for the sphere using $F_H = 6.6E\text{-}7$ m^3 and $F_E = 6.93E\text{-}7$ m^3, respectively. The theoretical estimate for the given metallic needle is 5.15E-7 m^3 yielding a ~25 % agreement. Comparing the measured F_E for the sphere with the dielectric formula suggests a dielectric constant of ~19.7.

BEAM TUBE RESONANCES

The HOMs in the ERL cavity are damped with ferrite rings connected to the cavity by beam tube sections, adding a length of 52.5 cm upstream and 55 cm downstream. The addition of the beam tubes complicates the search and identification of HOM resonances by adding new resonances or by changing the frequency of some cavity modes. The beam tube diameter of 24 cm was chosen to allow wave propagation from cavity to the damper while filtering the fundamental mode. Beam tube resonances are possible above cut-off for TE_{11}, TM_{01}, TE_{21}, and TM11 & TE_{01} at 732, 957, 1215, and 1559 MHz respectively. Being connected to the ferrite provides strong damping of the beam tube resonances proper. However, the possibility for high-Q end cell resonances exists above cut-off for the corresponding beam tube mode.

The search for the HOMs in the cavity proper of the ERL is best performed by S_{21} measurements between the Fundamental Power Coupler (FPC) and the Pick up (PU) probe, but it is precluded in the operational configuration. Search measurements are thus done between the up and down stream beam position monitors (BPM) and for the beam tube modes between two probes in one BPM. Mode identifications are done by bead pulling in the model and are completed by the comparison of data from the ERL with the copper model and MWS runs.

The ERL data in the frequency region from 0.7 to 1.25 GHz taken between the BPMs of the ERL are show in Fig. 7 The beam tube modes in the "empty" frequency regions between the fundamental and the first dipole passband and also the one between the second dipole and first quadrupole passband are listed in Table IV and will be investigated in this Section .

Table IV: Beam tube resonances in the ERL

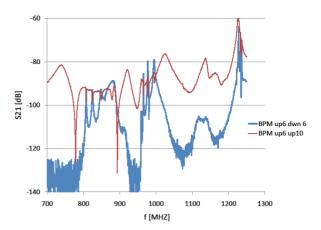| f [MHz]	Q
739	30
886	147
921	79
1024	48
1141	87

FIG. 7: S_{21} Transmission between FPC and PU in ERL.

Beam Tube Modes from 710 to 790 MHz

As discussed in Section II, establishing the fields by bead measurement requires a reasonably shaped S_{21} resonance curve. For this, the beam tube resonances are best excited by two BPM buttons in the ERL and by probes placed locally into the copper model beam tube. The S_{21} transmission in the 710 - 790 MHz region is shown in Fig. 8 for the Normal Conducting (NC) ERL, the model with (MDL w FRT) and without ferrite (MDL wo. FRT) dampers.
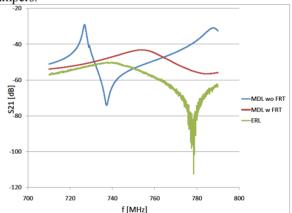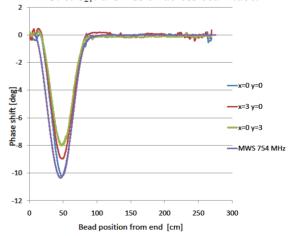

FIG. 8: S_{21} transmission across beam tube.

FIG. 9: Phase shift in TE_{111} due to bead pulling.

The beam tube resonance at 754 MHz has a $Q \approx 38$ and can be identified in the copper model. The resonance frequency in the model depends on beam tube length and ferrite parameters. Removal of the ferrite implies an effective length change and results in a significant frequency change, but retains the field character of a TE_{111} resonance. The perturbation measurement was done with a 1.27 cm dia. dielectric sphere pulled across the model on the axis, horizontally displaced by 3 cm, and vertically displaced by 3 cm. The results are shown in Fig. 9 and confirm the TE_{111} field pattern.

Beam Tube Modes from 1000 to 1200 MHz

The S21 transmission between two probes in the copper model beam tube is shown in Fig. 10 and that across the cavity is shown in Fig. 11. HOM identification by comparing the copper model data with that from the ERL is not obvious. The 1024 MHz resonance in the ERL may be identified with one at 1031 MHz in the copper model without ferrite, although this mode apparently is fully suppressed by the ferrite. Bead pulling with the needle on the axis and then horizontally and vertically displaced allows the mode identification. The positive phase change is explained as the result of using a metallic needle that is sensitive to electric as well as and magnetic fields. The horizontal bead pull data in Fig 12. together with the MWS curves identifies the resonance at 1024 MHz as a TE_{114} beam tube mode.
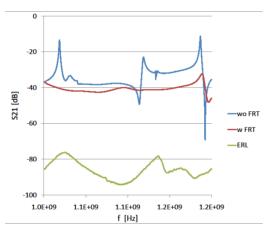

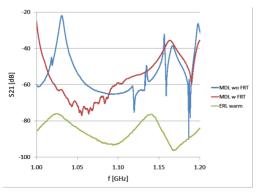FIG. 10: S21 transmission across ERL.
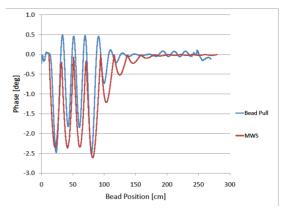

FIG. 11: S21 transmission across beam tube.

FIG. 12: Bead pulls (blue) and MWS data (red) for the TE_{114} mode at 1.024 GHz.

BEAD PULL MEASUREMENTS IN THE DIPOLE GROUP

Bead measurements were applied to the 10 HOMs in the two lowest bands in the frequency region from 800 to 1000 GHz. In order to analyze the field structure of a given HOM, several off-axis bead-pull sweeps must be taken at different measurement angles. The result for such a measurement (taken 4 cm off-axis) is shown in Fig. 13 for the 958.92 MHz mode. This resonance was first observed in MWS simulation at 957.81 MHz as a "trapped" dipole without fields coupling into the beam tubes. All 5 cells are clearly visible in the plot, with the strongest coupling in the center cell as expected for a trapped mode.
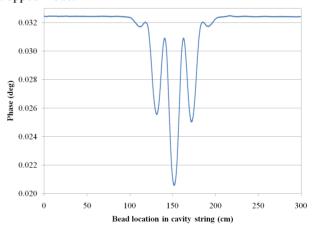

FIG. 13: S21 sweep data in the Cu model for the 958.92 MHz HOM, as measured across the cavity.

As noted in the equation above, the phase offset within a cell is directly related to the strength of E and H fields present and can be calculated by subtracting the maximum phase offset from the background (taken from a line fit to the outer points in Fig. 13 where the perturbation is not present in the cells). As the measurement angle changes, the maximum phase offset within a single cell correspondingly varies based on the HOM field structure, and this information can be used to identify the mode type (dipole, quadrupole, etc.). The

result for the 958.92 MHz mode is shown in Fig. 14. The phase offsets peak every 180°, indicating a clear dipole.
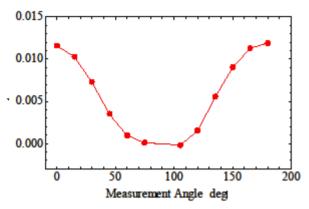

FIG. 14: Phase offset data for 958.92 MHz HOM.

Another direct comparison can be made between the data and the MWS output to determine if the measured dipole is the same dipole mode solution given by simulation. As a post processing step, the longitudinal electric field for the MWS dipole was computed at a distance of 4 cm off-axis down the length of the entire cavity string. This distance corresponds to the bead-pull measurement distance, and the angle for the calculation was chosen as that of the maximum E-field plane. For a simple comparison, the measurement data (using the sweep data at an angle for maximum E, 180°) was scaled so that the center cell peak magnitudes were aligned, and the result is shown in Fig. 15. The relative field strengths in each of the 5 cells agree very well in this comparison, leading us to conclude that the measured mode and the MWS result are in fact the same dipole resonance.
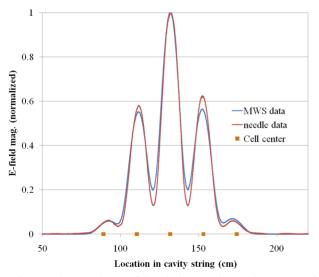

FIG. 15: Comparison of bead data and MWS output of normalized E_X field for the 958.92 MHz HOM.

BEAD PULL MEASUREMENTS IN THE QUADRUPOLE GROUP

The 1.22 GHz mode shown above in Table I is the first in a family of 5 resonances between 1.215 and 1.24 GHz. The correlation between these modes in the niobium ERL cavity at NC temperature and the copper prototype is very good, as shown in Fig. 16.
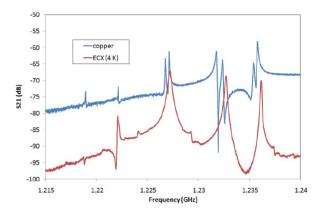

FIG. 16: Comparison of copper and niobium-cavity.

Some of the copper-cavity modes in the plot exhibit "splitting", a condition where an asymmetry in the cavity (namely, a slightly elliptical rather than circular shape) causes 2 distinct polarizations of a mode to occur around the normal resonant frequency. A comparison between center frequencies for the HOMs between the cavities is shown in Table V. The center frequency for the split HOMs was used in the calculation. MWS also predicts group of 5 quadrupoles at this frequency, with the lowest occurring at 1.218 GHz.

Table V: Comparison of niobium and copper cavity HOM frequencies in the 1.22 -1.24 GHz range.

Nb freq. [GHz] @ 4 K	Cu freq. [GHz]
1.22008	1.21984
1.22336	1.22215
1.22859	1.22700
1.23409	1.23195
1.23748	1.23568

Field structure for the 1.219 GHz mode was measured using the bead-pulling technique. In order to sufficiently couple to the resonance, S_{21} was measured across the center cell and an adjacent cell. The phase offset result is shown in Fig. 17. From the plot, it appears that the offset repeats every 90°, characteristic of a quadrupole mode.
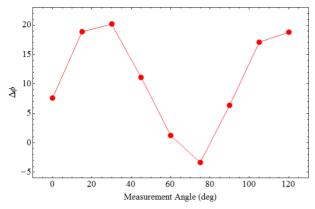
FIG. 17: Phase offset data for 1.2189 GHz HOM, showing quadrupole structure.

The comparison of measured and MWS E-field magnitudes for this quadrupole is shown in Fig. 18. The relative E-field magnitudes in the cells do vary appropriately, but the correspondence isn't as clear as the dipole case discussed above. A possible reason for this disparity is that the bead-pull data wasn't taken at a measurement angle for maximum E-field (which would be closer to 20°), while the MWS data is taken from this plane
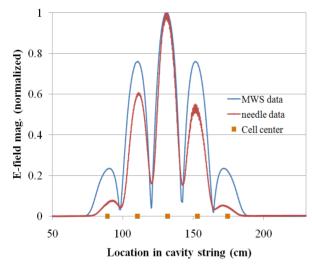

FIG. 18: Comparison of bead data and MWS of normalized EX field for the 1.2 GHz HOM.

Alternate Method

This quadrupole result matches that of a previous field structure measurement by an alternate method [7]. Small conducting probes were placed in holes drilled in cavity walls. The holes in the measured cell are located 45° apart, near the cell apex. While keeping the excitation probe in one whole and successively measuring phase at the other 7 holes, HOM structure can be determined by counting the number of 180° phase jumps. All 5 resonances in the 1.215-1.24 GHz range were found to have 4 phase changes, indicating quadrupole structure.

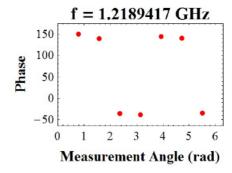The result for the 1.2189 (1.22008 in the ERL) GHz mode is shown in Fig. 19.

FIG. 19: Probe phase measurement data, showing 4 phase changes of 180°.

CONCLUSION

Identification of several low frequency HOMs in the ERL cavity was made possible for dipole modes, beam tube modes and quadrupole modes by matching their frequencies to corresponding resonance frequencies in the ferrite damped copper model. When matching is found, the electromagnetic field character is established by bead pulling and must be confirmed by MWS simulation runs.

Both, a metallic needle and a dielectric sphere were calibrated for bead pulling in the fundamental cavity mode and used for the other resonances. Bead pull measurements were done also for the select high-Q HOMs given in Table I in an attempt of their identification. The field character of these modes, with the sweep data for the 2.4599 GHz HOM shown in Fig. 20, is much more complex than in the modes analyzed above, preventing simple conclusions. Identification was prevented by several factors, among them the low Q of the model, the sensitivity of the needle to the magnetic as well as the electric field, and the failure to match the cavity and MWS resonance frequencies.
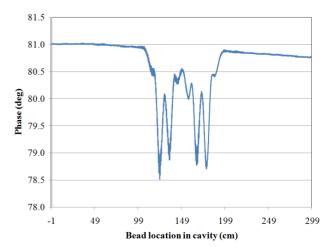

FIG. 20: Sweep data for the 2.4599 GHz HOM.

This R&D study was initiated to study the method and explore limitations of HOM identification and as such it established the basis for the forth coming measurements of the eRHIC cavity.

REFERENCES

[1] J. Müller, *Untersuchung über elektromagnetische Hohlräume.* Hochfrequenztechnik & Elektroakustik, **54**, p. 157-161 (1939).

[2] L. C. Maier, Jr.. and J. C. Slater, J. Appl. Phys., **23**, p. 68 (1952).

[3] L. C. Maier, *Field Strength Measurements in Resonant Cavities*, MIT-RLE-TR-143 (1949).

[4] H. Padamsee, J. Knobloch, and T. Hayes, *RF Superconductivity for Accelerators*, p. 137, (John Wiley & Sons, New York, 1998).

[5] H. Hahn and H. J. Halama, *Perturbation measurement of transverse R/Q in iris-loaded waveguides*, IEEE Trans. Microwave Theory and Techniques, vol. MTT-16, p. 20 (1968).

[6] R. Calaga, Ph. D. thesis, SUNY Stony Brook, 2006.

[7] E. C. Johnson, I. Ben-Zvi, H. Hahn, L. Hammons, and Wencan Xu, *Higher-Order Mode Analysis at the BNL Energy Recovery Linac*, Report C-AD, BNL-96110-2011-IR.